Electronic Supplementary Material (ESI) for Journal of Materials Chemistry C.
This journal is © The Royal Society of Chemistry 2018

Table of content

MOLECULAR STRUCTURE AND NAME OF DIFFERENT COMPOUNDS CITED IN THE TEXT

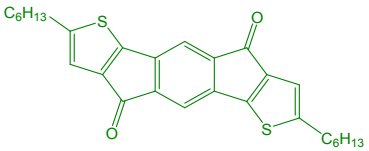

***para*-IDT(=O)$_2$**

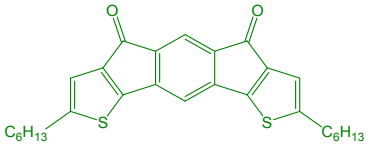

2,8-dihexyl-*s*-indaceno[1,2-*b*:7,6-*b*′]dithiophene-4,6-dione

***meta*-IDT(=O)$_2$**

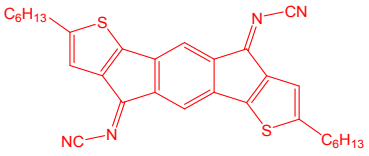

***para*-IDT(=NCN)$_2$**

(2,7-dihexyl-*s*-indaceno[1,2-b:5,6-b']bisthiophene--4,9-diylidene)dicyanamide

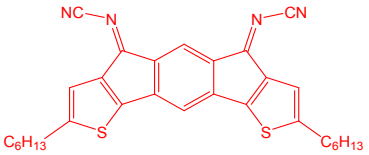

***meta*-IDT(=NCN)$_2$**

(2,8-dihexyl-*s*-indaceno[1,2-b:7,6-b']bisthiophene--4,6-diylidene)dicyanamide

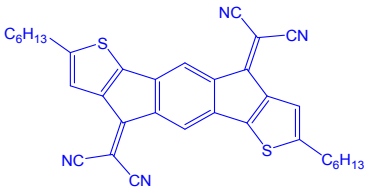

2,2'-(2,7-dihexyl-*s*-indaceno[1,2-*b*:5,6-*b*′]dithiophene-4,9-diylidene)dimalononitrile

***para*-IDT(=C(CN)$_2$)$_2$**

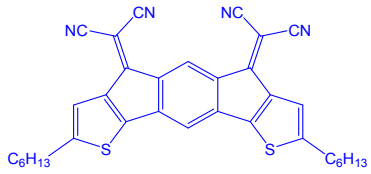

2,2'-(2,8-dihexyl-*s*-indaceno[1,2-*b*:7,6-*b*′]dithiophene-4,6-diylidene)dimalononitrile

***meta*-IDT(=C(CN)$_2$)$_2$**

Chart S1: Molecular structure, name and acronym of the different compounds cited in the publication (in red: molecules of the present work, in green and blue: molecules of previous work)

MATERIAL AND METHODS

Synthesis:

All manipulations of oxygen- and moisture-sensitive materials were conducted with a standard Schlenk technique. Commercially available reagents and solvents were used without further purification other than those detailed below. THF was distilled from sodium/benzophenone prior to use. Light petroleum refers to the fraction with boiling point 40-60°C. 2.5M solution of n-BuLi in hexane was purchased from Sigma Aldrich. 2,7-Dihexyl-4,9-dihydro-s-indaceno[1,2-*b:*5,6-b']dithiophene-4,9-dione and 2,8-dihexyl-s-indaceno[1,2-b:7,6-b']dithiophene-4,6-dione were synthesized according to published procedures with spectroscopic analyses and purity in perfect accordance with the literature.[1] Reactions were stirred magnetically, unless otherwise indicated. Analytical thin layer chromatography was carried out using aluminum backed plates coated with Merck Kieselgel 60 GF254 and visualized under UV light (at 254 and 360 nm). Chromatography was carried out using Teledyne Isco CombiFlash® Rf 400 (UV detection 200-360nm), over standard silica cartridges (Redisep® Isco, or Puriflash® columns Interchim). ^{1}H and ^{13}C NMR spectra were recorded using Bruker 300 MHz instruments (^{1}H frequency, corresponding ^{13}C frequency: 75 MHz); chemical shifts were recorded in ppm and J values in Hz. In the ^{13}C NMR spectra, signals corresponding to C, CH, CH_2 or CH_3 groups, assigned from DEPT, are noted, all others are C. The residual signals for the NMR solvent CD_2Cl_2 are: 5.32 ppm for the proton and 53.80 ppm for the carbon. The following abbreviations have been used for the NMR assignment: s for singlet, d for doublet, t for triplet and m for multiplet. High resolution mass spectra were recorded at the Centre Régional de Mesures Physiques de l'Ouest (CRMPO-Rennes) on Maxis 4G.

Electrochemical studies:

All electrochemical experiments were performed under an argon atmosphere, using a Pt disk electrode (diameter 1 mm), the counter electrode was a vitreous carbon rod and the reference electrode was a silver wire in a 0.1 M $AgNO_3$ solution in CH_3CN. Ferrocene was added to the electrolytic solution at the end of a series of experiments. The ferrocene/ferrocenium (Fc/Fc^+) couple served as internal standard. The three electrode cell was connected to a PAR Model 273 potentiostat/galvanostat (PAR, EG&G, USA) monitored with the ECHEM Software. Activated Al_2O_3 was added in the electrolytic solution to remove excess moisture. For a further comparison of the electrochemical and optical properties, all potentials are referred to the SCE electrode that was calibrated at 0.405 V *vs*. Fc/Fc^+ system. Following the work of Jenekhe,[1] we estimated the electron affinity (EA) or lowest unoccupied molecular orbital (LUMO) and the ionization potential (IP) or highest occupied molecular orbital (HOMO) from the redox data. Indeed, the LUMO level was calculated as: LUMO (eV)= -[E_{onset}^{red} (*vs* SCE) + 4.4] and the HOMO level as: HOMO (eV) = -[E_{onset}^{ox} (*vs* SCE) + 4.4], based on an SCE energy level of 4.4 eV relative to the vacuum. The electrochemical gap was calculated from : ΔE^{el} =|HOMO-LUMO| (in eV).

Molecular modeling :

Full geometry optimization with Density functional theory (DFT)[2-3] and Time-Dependent Density Functional Theory (TD-DFT) calculations were performed with the hybrid Becke-3 parameter exchange[4-6] functional and the Lee-Yang-Parr non-local correlation functional[7] (B3LYP) implemented in the Gaussian 09 (Revision B.01) program suite[8] using the default convergence criterion implemented in the program. The figures were generated with GaussView 5.0. DFT and TD-DFT calculations at the RB3LYP/6-311+g(d,p) in their respective optimized singlet state (optimization at the RB3LYP/6-311+g(d,p)) level of theory, infrared spectra were calculated on the final geometry to ascertain that a minimum was obtained *i.e.* no negative frequency). Calculations were carried out at the Centre Informatique National de l'Enseignement Supérieur (CINES) in Montpellier under project c2016085032.

Spectroscopic studies:

Cyclohexane (≥ 99.5 % AnalaR NORMAPUR®ACS, VWR chemicals), THF (≥ 99.5 % stabilized AnalaR NORMAPUR®ACS, VWR chemicals) and acetonitrile (CarloErba, anhydrous for analysis 99.8 %) were used without further purification. UV-visible spectra were recorded using a UV-Visible spectrophotometer SHIMADZU UV-1605. The optical gap was calculated from the absorption edge of the UV-vis absorption spectrum using the formula ΔE^{opt} (eV) = hc/λ, λ being the absorption edge (in meter). With h = 6.62606×10^{-34} J.s (1eV = 1.60217×10^{-19} J) and c = 2.99792×10^{8} m.s^{-1}, this equation may be simplified as: ΔE^{opt} (eV) = 1239.84/ λ (in nm).

Thermal analysis:

Thermal Gravimetric Analysis (TGA) were carried out with a Q50 apparatus of TA Instruments, at a scanning rate of 5 C min^{-1} and with air as purge gas. The transition temperatures and enthalpies were measured by differential scanning calorimetry (DSC) with a TA Instruments DSC-Q1000 instrument operated at a scanning rates of 1 to 5°C min^{-1} on heating and on cooling.

Self-organization properties:

The SAXS patterns were recorded with a linear monochromatic Cu Kα1 beam (λ = 1.5405 Å) obtained using a sealed-tube generator (600 W) equipped with a bent quartz monochromator. Patterns were recorded with a curved Inel CPS 120 counter gas-filled detector linked to a data acquisition computer; periodicities up to 70 Å can be measured, and the sample temperature controlled to within ±0.01 °C from 20 to 200 °C. The crude powder was filled in Lindemann capillaries of 1 mm diameter and 10 µm wall thickness and exposure times were varied from 1 to 24 h. The optical textures of the mesophases were studied with a Leitz polarizing microscope (POM) equipped with a Mettler FP82 hot-stage and an FP80 central processor.

X-Ray

Crystals were picked up with a cryoloop and then frozen at 150 K under a stream of dry N2on a APEX II Brucker AXS or a D8 VENTURE Bruker AXS diffractometer for X-ray data collection (Mo Kα radiation, λ = 0.71073 Å). Crystallographic data have been deposited with the Cambridge Crystallographic Data Centre as supplementary publication Data CCDC 1848046 for ***para*-IDT(=NCN)$_2$** and CCDC 1848047 for ***meta*-IDT(=NCN)$_2$**. Copies of the data can be obtained free of charge on application to CCDC, 12 Union Road, Cambridge CB2 1EZ, UK [fax: (+44) 1223-336-033; e-mail: deposit@ccdc.cam.ac.uk]. Figures were generated with Mercury software 3.7.

SYNTHESIS

General procedure for the synthesis of IDT(=NCN)$_2$ compounds

Bis(trimethylsilyl)carbodiimide (0.74 mL, 3.24 mmol) was added to a solution of $TiCl_4$ (0.42mL, 3.80 mmol) dissolved in dry CH_2Cl_2 (16 mL) at 0°C. The resulting mixture was stirred at this temperature for 1h and the corresponding ketone (500 mg, 1.08 mmol) dissolved in CH_2Cl_2 (40 mL) was added. The mixture was allowed to warm up to room temperature overnight. Water was then added (200 mL) and the mixture was extracted with CH_2Cl_2 (3 x 100 mL). The combined organic extracts were rinsed with water (2 x 200 mL), dried over anhydrous magnesium sulfate, filtered and concentrated under reduced pressure. The residue was recrystallized from hot CH_2Cl_2 with methanol.

***para*-IDT(=NCN)$_2$**

The general procedure was performed with ***para*-IDT(=O)$_2$** as starting material. After recrystallization, ***para*-IDT(=NCN)$_2$** was obtained as a grey-green powder with a yield of 57% (319 mg, 0.62 mmol).

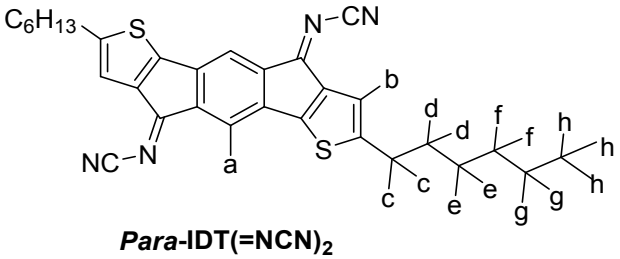

***Para*-IDT(=NCN)$_2$**

m.p. 139°C; ^{1}H NMR (300 MHz, 1,1,2,2-tetrachloroethane-D_2) δ 7.28 (s, 2H, Hb), 7.23 (s, 2H, Ha), 2.81 (t, *J* = 7.6 Hz, 4H, Hc), 1.69 (t, *J* = 7.4 Hz, 4H, Hd), 1.35 (m, 12H, He/Hf/Hg), 0.98 – 0.86 (m, 6H, Hh); ^{13}C NMR (75 MHz, CD_2Cl_2) δ 154.73 (C), 153.01 (C), 142.85 (C), 138.77 (C), 137.52 (C), 119.50 (CH), 114.95 (C), 114.46 (CH), 31.30 (CH_2), 31.16 (CH_2), 30.54 (CH_2), 28.48 (CH_2), 22.43 (CH_2), 14.04 (CH_3); HRMS calculated for $C_{30}H_{30}N_4NaS_2$: 533.1804, found:533.1803 $[M+Na]^{+,}$ elemental analysis calculated for $C_{30}H_{30}N_4S_2$: C, 70.55%; H, 5.92%; N, 10.97%; S, 12.55%. Found: C, 70.43%; H, 5.90%; N, 10.86%, S, 12.71%, IR (ATR, cm^{-1}): v= 418, 474, 490, 528, 552, 607, 621, 644, 661, 696, 742, 827, 856, 893, 939, 972, 1022, 1055, 1124, 1159, 1226, 1267, 1323, 1377, 1440, 1473, 1589, 1680, 1807, 2175 (CN), 2850, 2923, 3025, 3064

***meta*-IDT(=NCN)$_2$**

The general procedure was performed with ***meta*-IDT(=O)$_2$** as starting material. After recrystallization, ***meta*-IDT(=NCN)$_2$** was obtained as a brown powder with a yield of 73% (404 mg, 0.79 mmol).

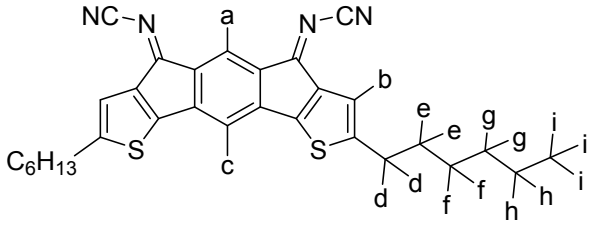

***Meta*-IDT(=NCN)$_2$**

m.p. 52°C; ^{1}H NMR (300 MHz, 1,1,2,2-tetrachloroethane-D_2) δ 7.58 (s, 1H, Ha), 7.33 (s, 2H, Hb), 6.90 (s, 1H, Hc), 2.85 (t, J = 7.6 Hz, 4H, Hd), 1.69 (d, J = 8.7 Hz, 4H, He), 1.51 – 1.16 (m, 12H, Hf/Hg/Hh), 1.05 – 0.75 (m, 6H, Hi); ^{13}C NMR (75 MHz, CD_2Cl_2) δ 176.15 (C), 155.03 (C), 151.93 (C), 146.16 (C), 139.34, 135.35 (C), 119.94 (CH), 119.02 (CH), 114.63 (C), 111.76 (CH), 31.30 (CH_2), 31.19 (CH_2), 30.71 (CH_2), 28.50 (CH_2), 22.42 (CH_2), 14.04 (CH_3); HRMS calculated for $C_{30}H_{31}N_4S_2$: 511.1985 found: 511.1988 $[M+H]^+$; elemental analysis calculated for $C_{30}H_{30}N_4S_2$: C, 70.55%; H, 5.92%; N, 10.97%; S, 12.55%. Found: C, 70,61%; H, 6.07%; N, 10.71%; S, 12.63%; IR (ATR, cm^{-1}): v= 418, 430, 474, 491, 540, 567, 604, 621, 642, 698, 719, 741, 827, 854, 889, 939, 1055, 1161, 1184, 1228, 1267, 1323, 1367, 1415, 1446, 1473, 1498, 1589, 2173 (CN), 2852, 2924, 2950

THERMAL PROPERTIES: TGA, DSC & SAX

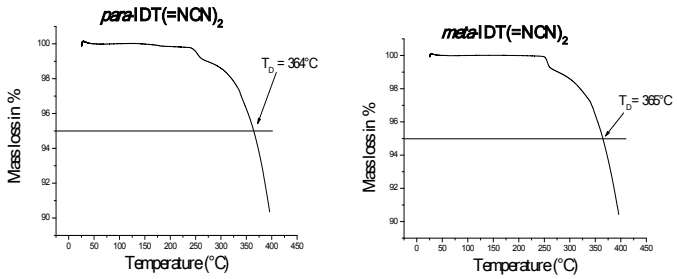

Figure S1: TGA of ***para*-IDT(=NCN)$_2$** (A) and ***meta*-IDT(=NCN)$_2$** (B)

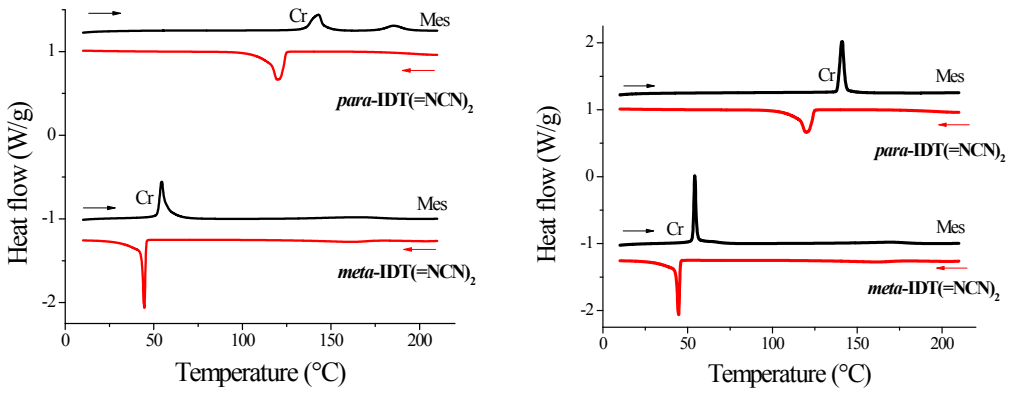

Figure S2: DSC traces of IDT(=NCN)$_2$ regioisomers (left: 1st heating run (black) and cooling run (red); right: 2nd cooling run (red) and heating run (black) at 5°C/min, endotherm up); Cr: crystalline phase; Mes: mesotropic phase

STRUCTURAL PROPERTIES

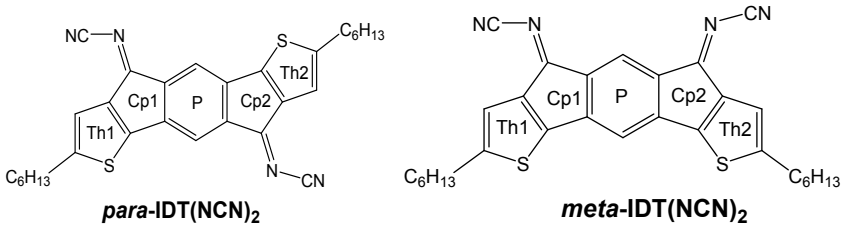

Figure S3: Numbering of the different rings for the **IDT** isomers

	Angle (°) between Th1 and P	Angle (°) between P and Th2
***Para*-IDT(=NCN)$_2$**	0.15	0.15
***Meta*-IDT(=NCN)$_2$**	2.00	1.20

Table S1: Measured values of some angles of interest within the **IDT(=NCN)$_2$** isomers skelettons

In ***meta*-IDT(=NCN)$_2$**, the indacenodithiophene core is not symmetrically bended. In fact, one of the thiophene rings forms an angle of 2.00° (Figure S 8) with the central phenyl ring and the second one forms an angle of 1.20° (Figure S 9).

This phenomenon can be explained by the different folding of each hexyl chain: the one attached to Th1 being folded directly from the attached carbon atom with a torsion angle of 81.93° and the other one, attached to Th2, with a torsion angle of 17.04°.

There are short contacts along the a axis and along the b axis. The former leads to a parallel cofacial alterned packing and the latter to edge on packing.

***Para*-IDT(=NCN)$_2$**

Identification code	shelx
Empirical formula	$C_{30}H_{30}N_4S_2$
Formula weight	510.70
Temperature	296(2) K
Wavelength	0.71073 Å
Crystal system	Triclinic
	P -1
	a = 4.8961(4) Å ; α= 91.827(3)°.
	b = 8.3384(7) Å ; β= 90.314(3)°.
Space group Unit cell dimensions	c = 16.1441(14) Å ; γ = 99.320(3)°.
Volume	650.02(9) Å^3
Z	1
Density (calculated)	1.305 Mg/m^3
Absorption coefficient	0.232 mm^{-1}
F(000)	270
Crystal size	N/A
Theta range for data collection	2.477 to 27.507°.
Index ranges	-4<=h<=6, -10<=k<=8, -15<=l<=20
Reflections collected	6582
Independent reflections	2965 [R(int) = 0.0320]
Completeness to theta = 25.242°	99.9 %
Refinement method	Full-matrix least-squares on F^2
Data / restraints / parameters	2965 / 0 / 164
Goodness-of-fit on F2	1.030
Final R indices [I>2sigma(I)]	R1 = 0.0444, wR2 = 0.0858
R indices (all data)	R1 = 0.0717, wR2 = 0.0965
Extinction coefficient	n/a
Largest diff. peak and hole	0.340 and -0.307 e.Å-3

Table S 2: Crystal data and structure refinement for ***para*-IDT(=NCN)$_2$**

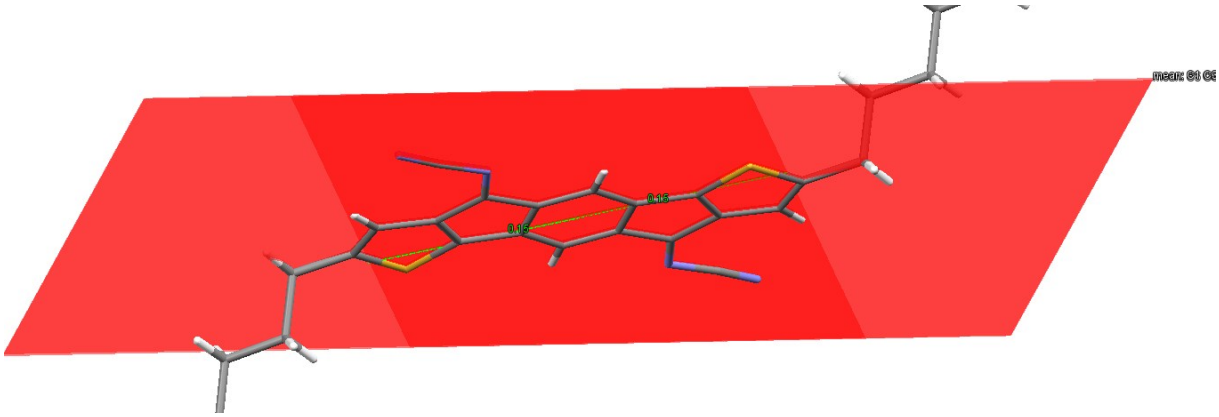

Figure S 4: Angles between the phenyl and both thiophene rings: 0.15° in ***para*-IDT(=NCN)$_2$**

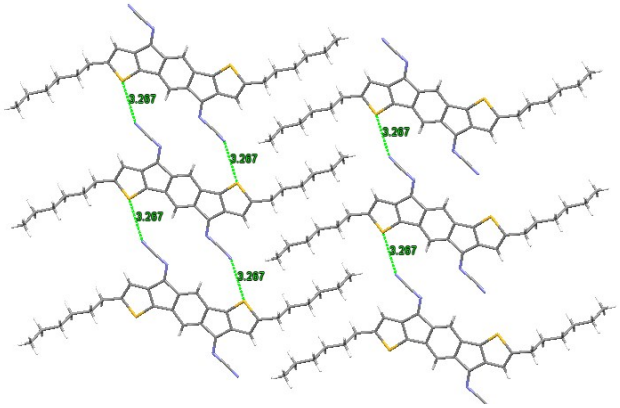

Figure S 5: Short N/S intermolecular distances in the ***para*-IDT(=NCN)$_2$** packing

Some short N/S intermolecular distances are observed ($d_{N/S}$=3.27 Å) in the ***para*-IDT(=NCN)$_2$** packing. These short distances are shorter than the sum of the Van der Walls radii, ie $d_{C/H}$=3.35 Å)

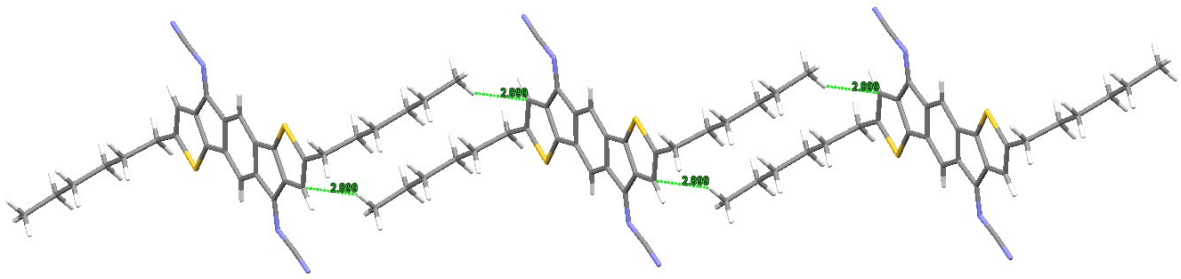

Figure S 6: Some short C/H intermolecular distances are observed ($d_{C/H}$=2.89 Å) in the ***para*-IDT(=NCN)$_2$** packing. These short distances are shorter than the sum of the Van der Walls radii, ie d=2.90 Å

***Meta*-IDT(=NCN)$_2$**

Identification code	shelx
Empirical formula	C30 H30 N4 S2
Formula weight	510.70
Temperature	150(2) K
Wavelength	71.073 pm
Crystal system	Triclinic
Space group	P -1
Unit cell dimensions	a = 702.93(11) pm ; α= 81.078(5)°.
	b = 1008.18(13) pm ; β= 85.447(6)°.
	c = 1897.2(3) pm ; γ= 80.052(5)°.
Volume	1.3064(3) nm^3
Z	2
Density (calculated)	1.298 Mg/m^3
Absorption coefficient	0.231 mm^{-1}
F(000)	540
Crystal size	N/A
Theta range for data collection	2.176 to 27.499°.
Index ranges	-9<=h<=9, -11<=k<=13, -24<=l<=24
Reflections collected	27333
Independent reflections	5978 [R(int) = 0.1233]
Completeness to theta = 25.242°	100.0 %
Refinement method	Full-matrix least-squares on F2
Data / restraints / parameters	5978 / 0 / 328
Goodness-of-fit on F2	1.051
Final R indices [I>2sigma(I)]	R1 = 0.0601, wR2 = 0.1424
R indices (all data)	R1 = 0.1015, wR2 = 0.1698
Extinction coefficient	0.034(5)
Largest diff. peak and hole	0.692 and -0.776 $e.Å^{-3}$

Table S 3: Crystal data and structure refinement for ***meta*-IDT(=NCN)$_2$**

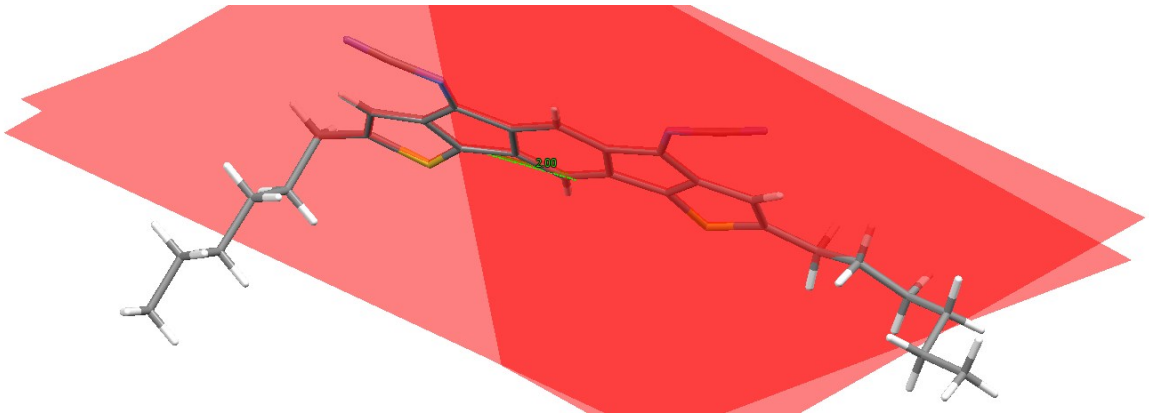

Figure S 7: Angle between cycle Th1 and Ph: 2.00° in ***meta*-IDT(=NCN)$_2$**

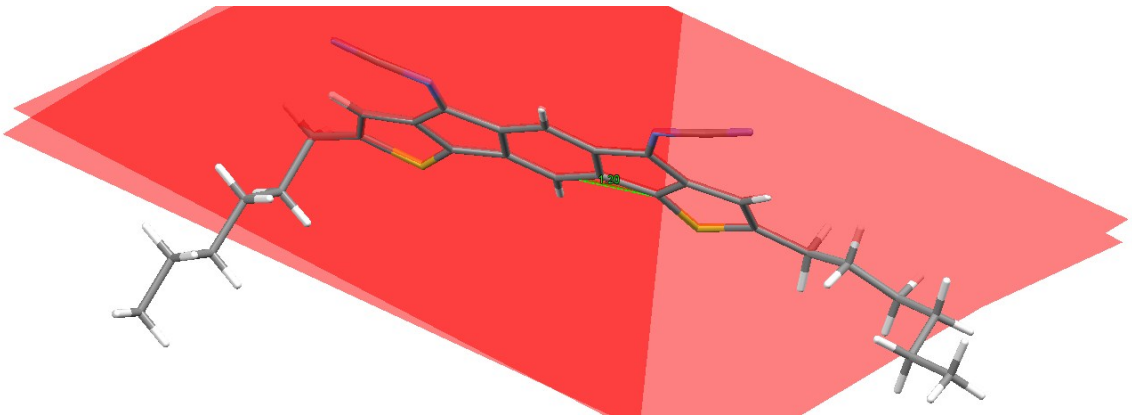

Figure S 8: Angle between cycles Ph and Th_2: 1.20° in ***meta*-IDT(=NCN)$_2$**

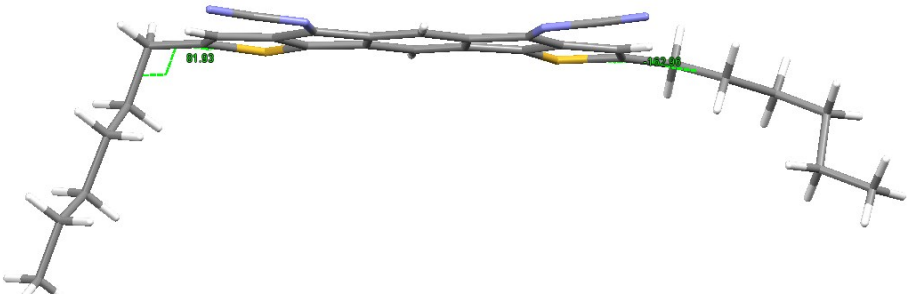

Figure S 9: Angle between Th1 and its attached hexyl chain: 81.93° and between Th2 and its attache hexyl chain: 17.04° (180-162.96)in ***meta*-IDT(=NCN)$_2$**

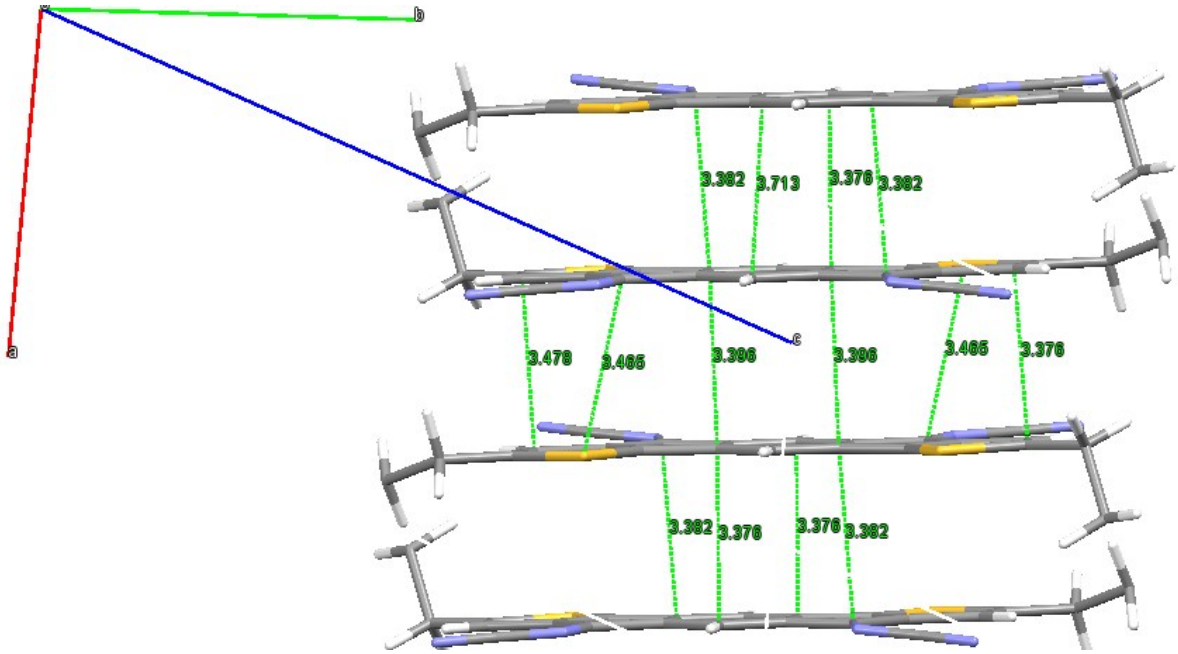

Figure S 10: Some short C/C and C/S intermolecular distances are observed ($d_{C/C}$=3.38 Å, $d_{C/C}$=3.39 Å, $d_{C/S}$=3.47 Å) along the a axis in the ***meta*-IDT(=NCN)$_2$** packing. These short distances are shorter than the sum of the Van der Walls radii, ie $d_{C/C}$=3.40 Å, $d_{C/S}$=3.50 Å). The 4 last atoms attached to the alkyl chains have been removed for clarity.

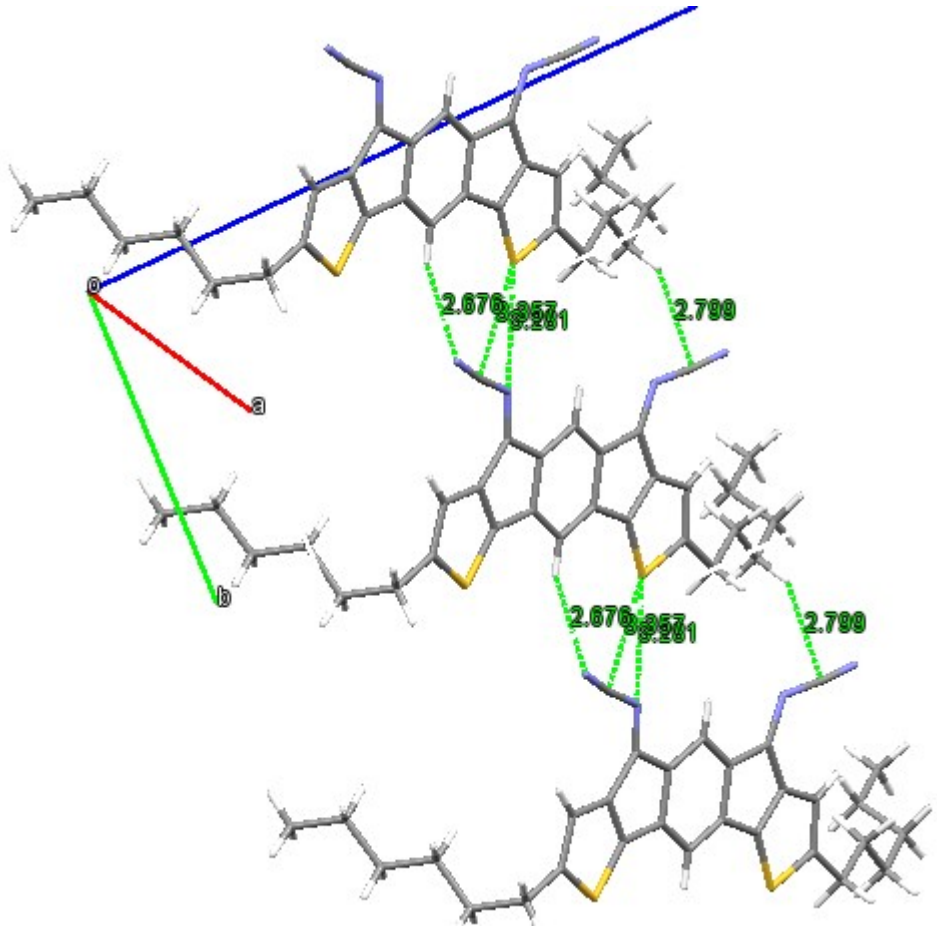

Figure S11. Some short N/H and N/S, C/S and C/H intermolecular distances are observed ($d_{N/H}$=2.68 Å, $d_{N/S}$=3.28 Å, $d_{C/S}$=3.36 Å, $d_{C/H}$=2.90 Å) along the b axis in the ***meta*-IDT(=NCN)$_2$** packing. These short distances are shorter than the sum of the Van der Walls radii, ie $d_{N/H}$=2.75 Å, $d_{N/S}$=3.35 Å, $d_{C/S}$=3.50 Å, $d_{C/H}$=2.90 Å).

Determination of the interactions strength between IDT rings in *para*-IDT(=NCN)$_2$ using Janiak criteria[9-13]

One may note that, as depicted between green and orange molecules (Figure S12), the inter-planar distance between two *para*-IDT cores is very short, 3.41 Å. In order to go deeper in the knowledge of these interactions, we measured for the rings of each IDT in interaction with the other one (rings 1 and 2, 3 and 4 and 5 and 6) the distance $d_{cent-cent}$ between their centroid and we calculate the vertical displacement (3.51 Å) and the ring slippage angles. As discussed by Janiak[9] these parameters can provide relevant information on the strength of the interactions between two phenyl rings. The $d_{cent-cent}$ values are 3.61 Å for rings 1/2 or 5/6 and of 3.52 Å for rings 3/4, the vertical displacements are of 1.17 Å for rings 1/2 or 5/6 and of 0.85 Å for rings 3/4 and the ring slippage angles are of 18.96 ° for rings 1/2 or 5/6 and of 14.35 ° for rings 3/4. In the light of Janiak's works, which show that strong interactions are pointed by dC-C values <3.8 Å, vertical displacements<1.5 Å, and ring slippage angles (<25°), we conclude that the two green and orange IDT cores are in strong interactions thanks to the interactions between rings 1/2, 3/4 and 5/6.

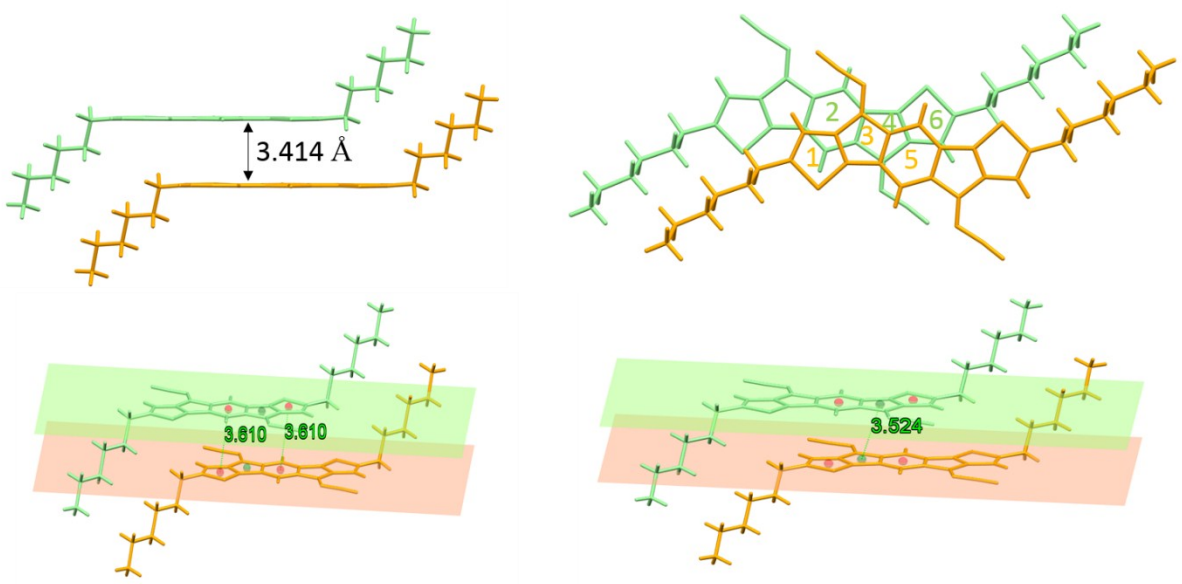

$d_{P1/P2}$: 3.414 Å $d_{C1/C2}$ and $d_{C5/C5}$: 3.610 Å, d_{vert}: 1.1733 Å => slippage angle: 18.96 °

$d_{C3/C4}$: 3.524 Å, , d_{vert}: 0.847 Å => slippage angle: 14.35 °

Figure S12. Arrangement of two ***para*-IDT(=NCN)$_2$** molecules (green and orange) in the packing diagram.

Determination of the interactions strength between IDT rings in *meta*-IDT(=NCN)$_2$ using Janiak criteria[9-13]

Between red and grey IDT cores: the dC-C values are 3.558 Å for rings 1/2 or 5/6 and of 3.555 Å for rings 3/4, the vertical displacements are of 1.16 Å for rings 1/2 or 5/6 and of 1.15 Å for rings 3/4 and the ring slippage angles are of 19.05 ° for rings 1/2 or 5/6 and of 18.91 ° for rings 3/4 whereas between red and blue IDT cores the values were of 3.618 Å for rings 1/7 or 5/9 and of 3.616 Å for rings 3/8, the vertical displacements are of 1.13 Å for rings 1/7 or 5/9 and of 1.308 Å for rings 3/8 and the ring slippage angles are of 21.29 ° for rings 1/7 or 5/9 and of 21.21 ° for rings 3/8. Those values are in accordance with the Janiak criteria describing π systems in strong interactions, one may note that interaction are even slightly stronger between red and grey molecules than between the red and blue ones (Figure S13).

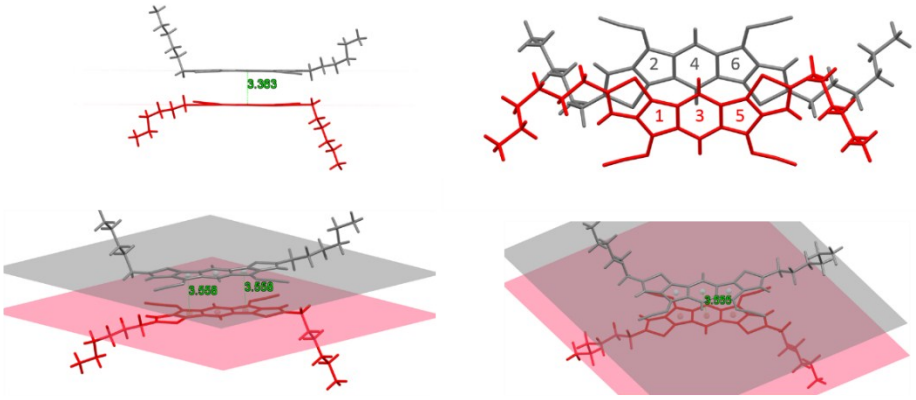

$d_{P1/P2}$: 3.363 Å $d_{C1/C2}$ and $d_{C5/C5}$: 3.558 Å, d_{vert}: 1.1617 Å => slippage angle: 19.05 °

$d_{C3/C4}$: 3.555 Å, d_{vert}: 1.15249 Å => slippage angle: 18.91 °

Figure S13: Arrangement of two red and grey ***meta*-IDT(=NCN)$_2$** molecules in the packing diagram.

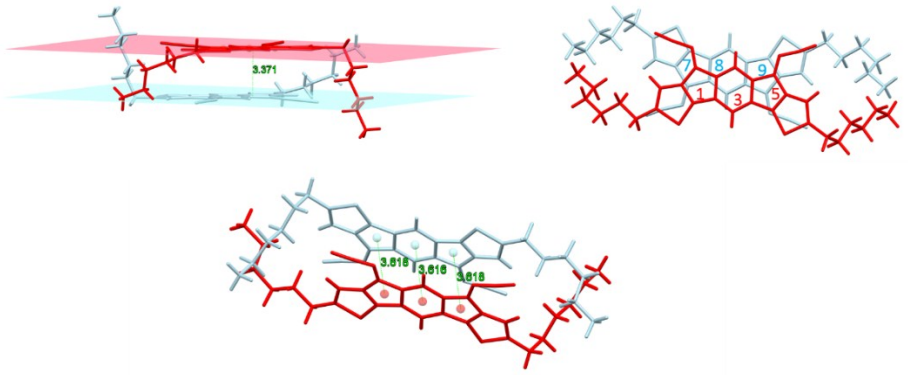

$d_{P1/P3}$: 3.371 Å $d_{C1/C7}$ and $d_{C5/C9}$: 3.618 Å, d_{vert}: 1.1314 Å => slippage angle: 21.29 °

$d_{C3/C8}$: 3.616 Å, , d_{vert}: 1.308 Å => slippage angle: 21.21 °

Figure S14: Arrangement of two red and blue ***meta*-IDT(=NCN)$_2$** molecules in the packing diagram.

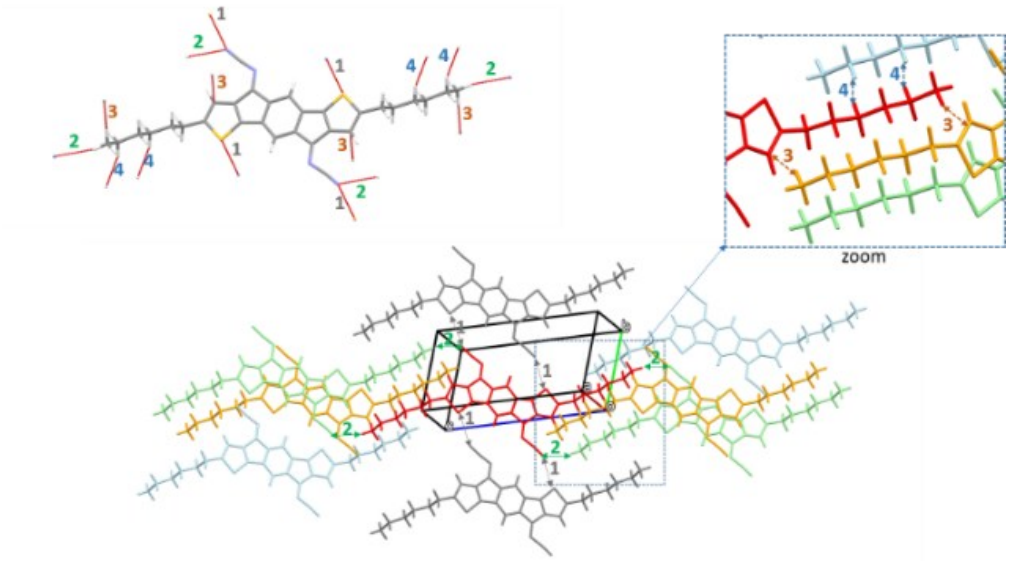

Figure S15: Intermolecular short contacts in ***para*-IDT(=NCN)$_2$**

Each molecule of ***para*-IDT(=NCN)$_2$** is surrounded by eight molecules with 16 atoms displaying short intermolecular distances. If one considers one molecule (colored in red in Figure S14), there are four short S-N contacts (labelled 1, d_{S-N}=3.26 Å, sum of the Van der Waals radii= 3.35 Å) with the two molecules colored in grey, four short N-H contacts (labelled 2, d_{N-H}= 2.71 Å, sum of the Van der Waals radii = 2.75 Å) with two molecules colored in green, four short C-H contacts (labelled 3, d_{C-H}= 2.89 Å, sum of the Van der Waals radii = 2.9 Å) with two molecules colored in orange (see zoom in Figure 3) and four short H-H contacts (labelled 4, d_{H-H}=2.37 Å, sum of the Van der Waals radii=2.40 Å) with two molecules colored in blue (see zoom in Figure S14). Thus, each of the eight surrounding molecule is involved in two short contacts with the central molecule showing the strength of this organization.

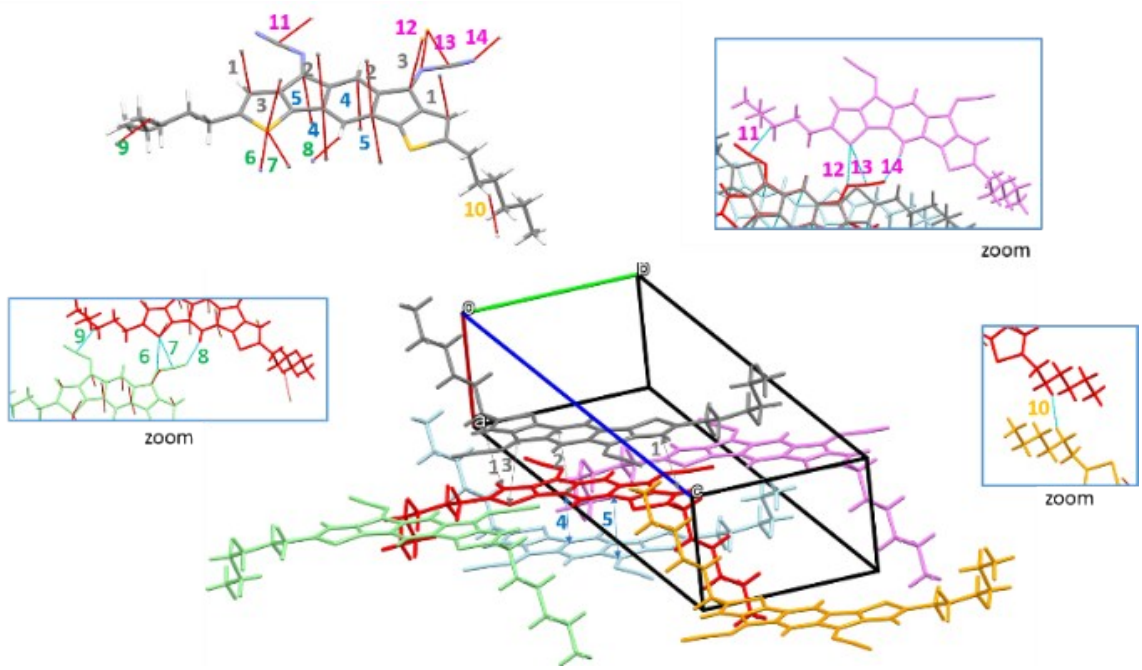

Figure S16: Intermolecular short contacts in ***meta*-IDT(=NCN)$_2$**

Each ***meta*-IDT(=NCN)$_2$** molecule (colored in red Figure S15) is surrounded by five other molecules with 19 atoms displaying short intermolecular contacts. Thus, four short C-C contacts (two labelled **1**, $d_{C\text{-}C}$=3.37 Å, and two labelled **2**, $d_{C\text{-}C}$= 3.39 Å, sum of the Van der Waals radii= 3.4 Å) and two short C-S contacts (labelled **3**: $d_{C\text{-}S}$=3.46 Å, sum of the Van der Waals radii= 3.5 Å) are detected with the molecule colored in grey. Four other short $d_{C\text{-}C}$ are also detected with molecule colored in blue (two labelled **4**, $d_{C\text{-}C}$= 3.37 Å and two labelled **5**, $d_{C\text{-}C}$= 3.38 Å, sum of the Van der Waals radii = 3.4 Å). Four other short contacts: S-N (labelled **6**, $d_{S\text{-}N}$ =3.28 Å, sum of the Van der Waals radii = 3.35 Å), S-C (labelled **7**, $d_{S\text{-}C}$ = 3.35 Å sum of the Van der Waals radii=3.5 Å), N-H (labelled **8**, $d_{N\text{-}H}$ =2.67 Å sum of the Van der Waals radii= 2.75 Å) and C-H (labelled **9**, $d_{C\text{-}H}$ 2.79 Å sum of the Van der Waals radii=2.9 Å) are also noticed between with the molecule colored in green. The hexyl chains also lead to one short H-H contact with the molecule colored in orange (labelled **10**, $d_{H\text{-}H}$=2.37 Å, sum of the Van der Waals radii= 2.4 Å). Finally, four short contacts (labelled **11**: $d_{C\text{-}H}$=2.8 Å, sum of the Van der Waals radii=2.9 Å, **12**: $d_{S\text{-}N}$ =3.28 Å, sum of the Van der Waals radii = 3.35 Å, **13**: $d_{S\text{-}C}$ = 3.36 Å sum of the Van der Waals radii=3.5 Å and **14**: $d_{N\text{-}H}$ =2.68 Å sum of the Van der Waals radii= 2.75 Å) are detected with the molecule colored in purple.

THEORETICAL MODELING

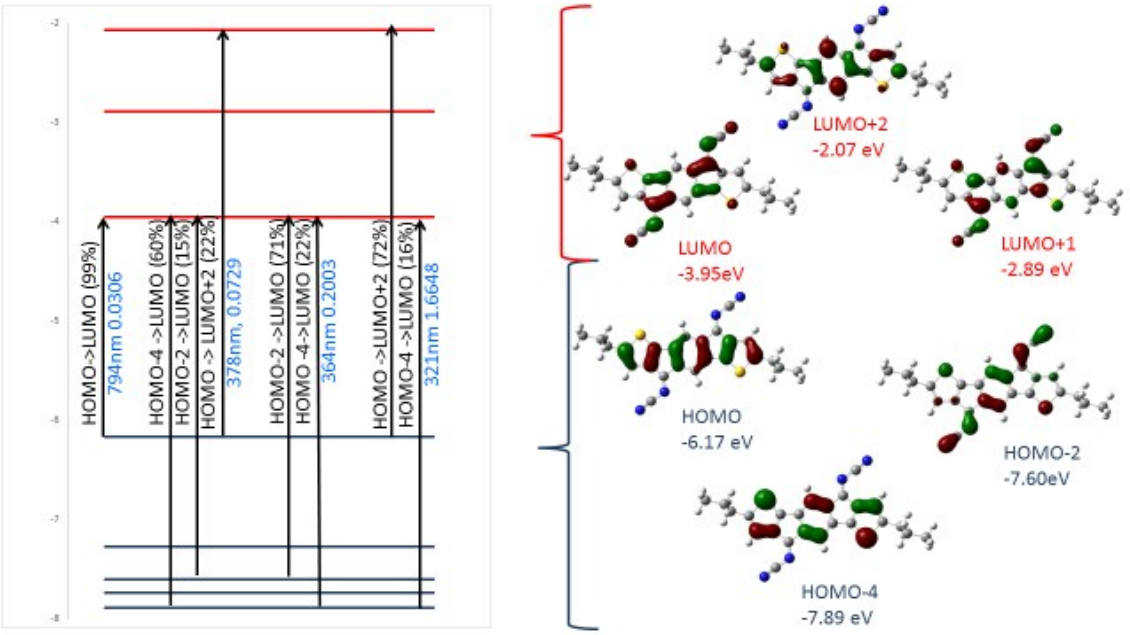

Figure S 17: Calculated frontier molecular orbitals by DFT and four electronic transitions of interest calculated by TD-DFT of ***para-* IDT(=NCN)$_2$**, after geometry optimization with DFT B3LYP/6-311G+(d,p), shown with a cut-off 0.04

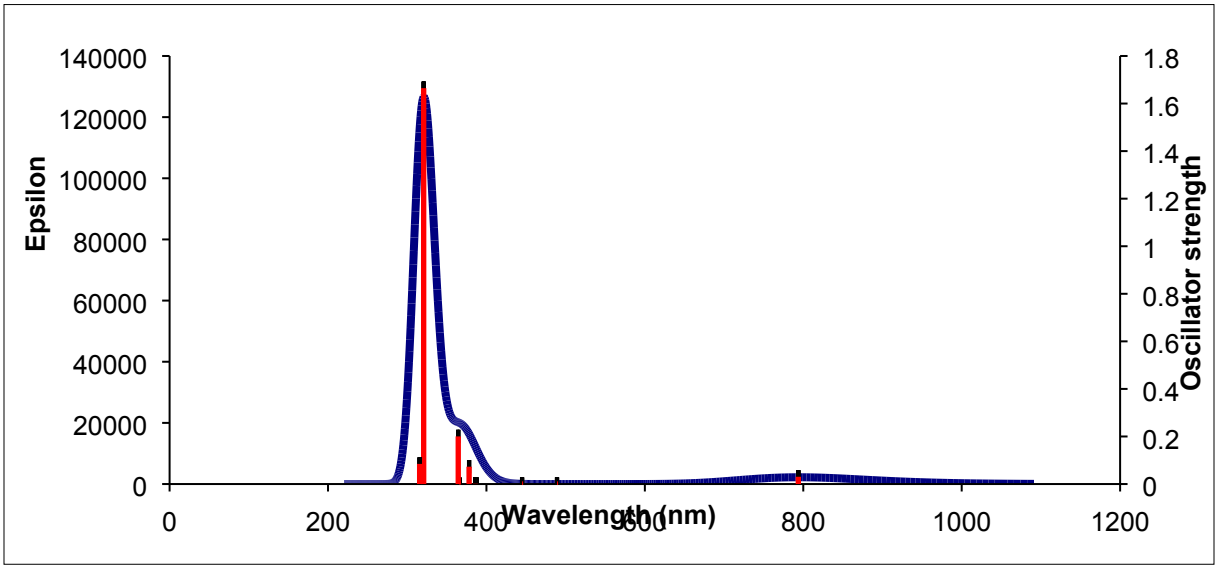

Figure S 18: Predicted UV-vis spectra from TD-DFT energy calculations of ***para*-IDT(=NCN)$_2$** after geometry optimization with DFT B3LYP/6-311 G+(d,p).

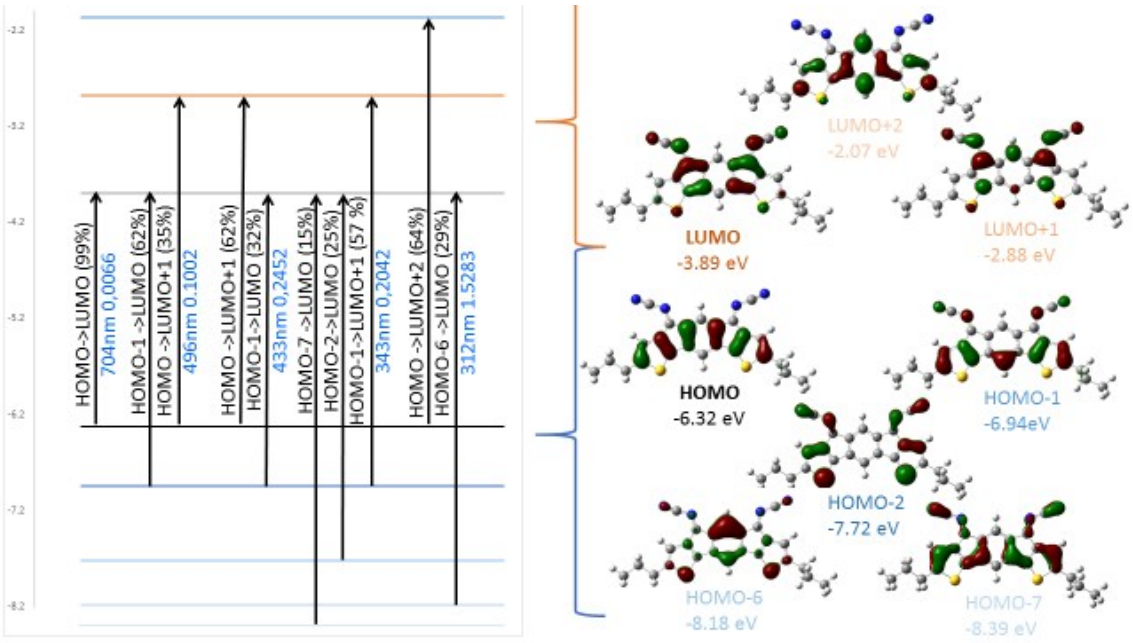

Figure S 19: Calculated frontier molecular orbitals by DFT and five electronic transitions of interest calculated by TD-DFT of ***meta*-IDT(=NCN)$_2$**, after geometry optimization with DFT B3LYP/6-311G+(d,p), shown with a cut-off 0.04

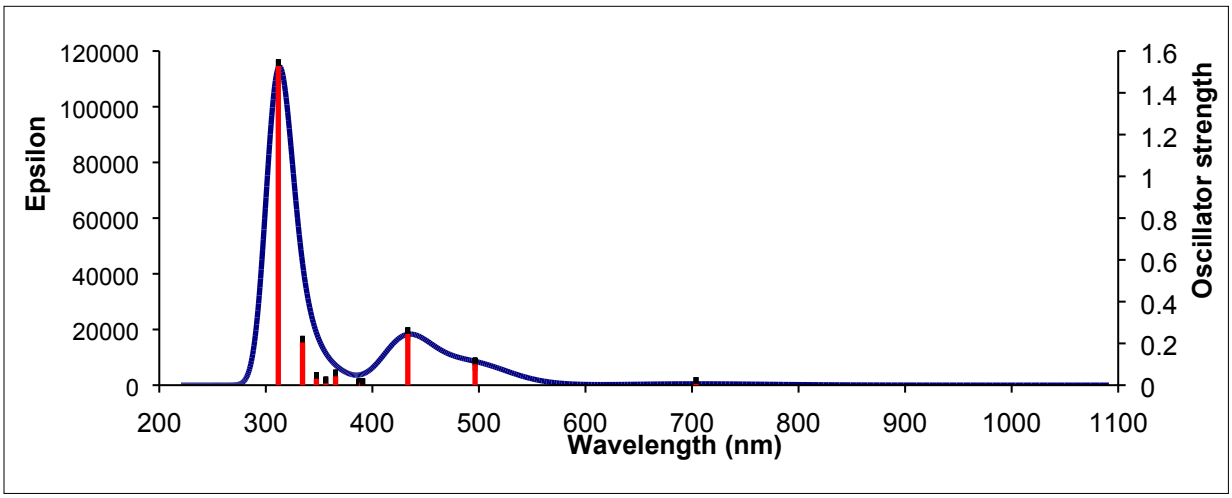

Figure S 20: Predicted UV-vis spectra from TD-DFT energy calculations of ***meta*-IDT(=NCN)$_2$** after geometry optimization with DFT B3LYP/6-311 G+(d,p).

ORGANIC FIELD-EFFECT TRANSISTOR STRUCTURES

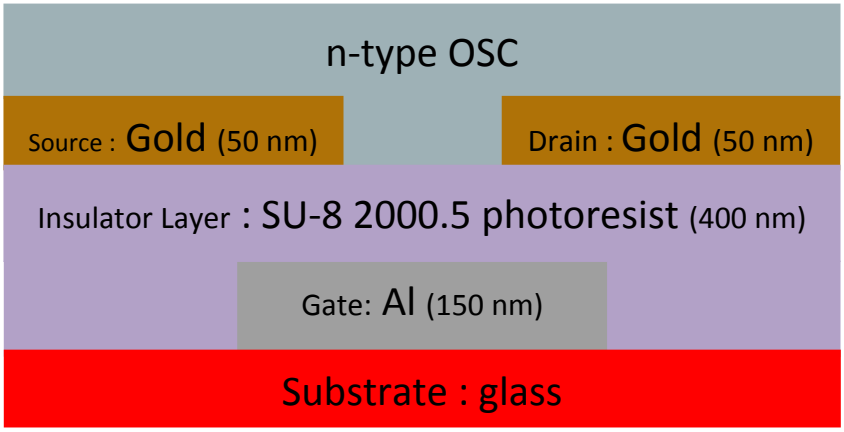

Figure S 21: Stucture of the bottom-gate bottom-contact n-type channel OFETs: on glass substrate

The fabrication process is described as follows: 150 nm thick aluminium layer was evaporated and patterned by conventional photolithography on a 5x5 cm² rigid glass substrate. Then, SU-8 2000.5 Photoresist from Microchem[14] was then spin-coated in order to obtain a 400 nm thick layer. 50 nm thick gold layer was then thermally evaporated and patterned by photolithography. Finally, the OSCs were deposited by evaporation under vacuum as a 40 nm thick layer.

COPIES OF NMR SPECTRA

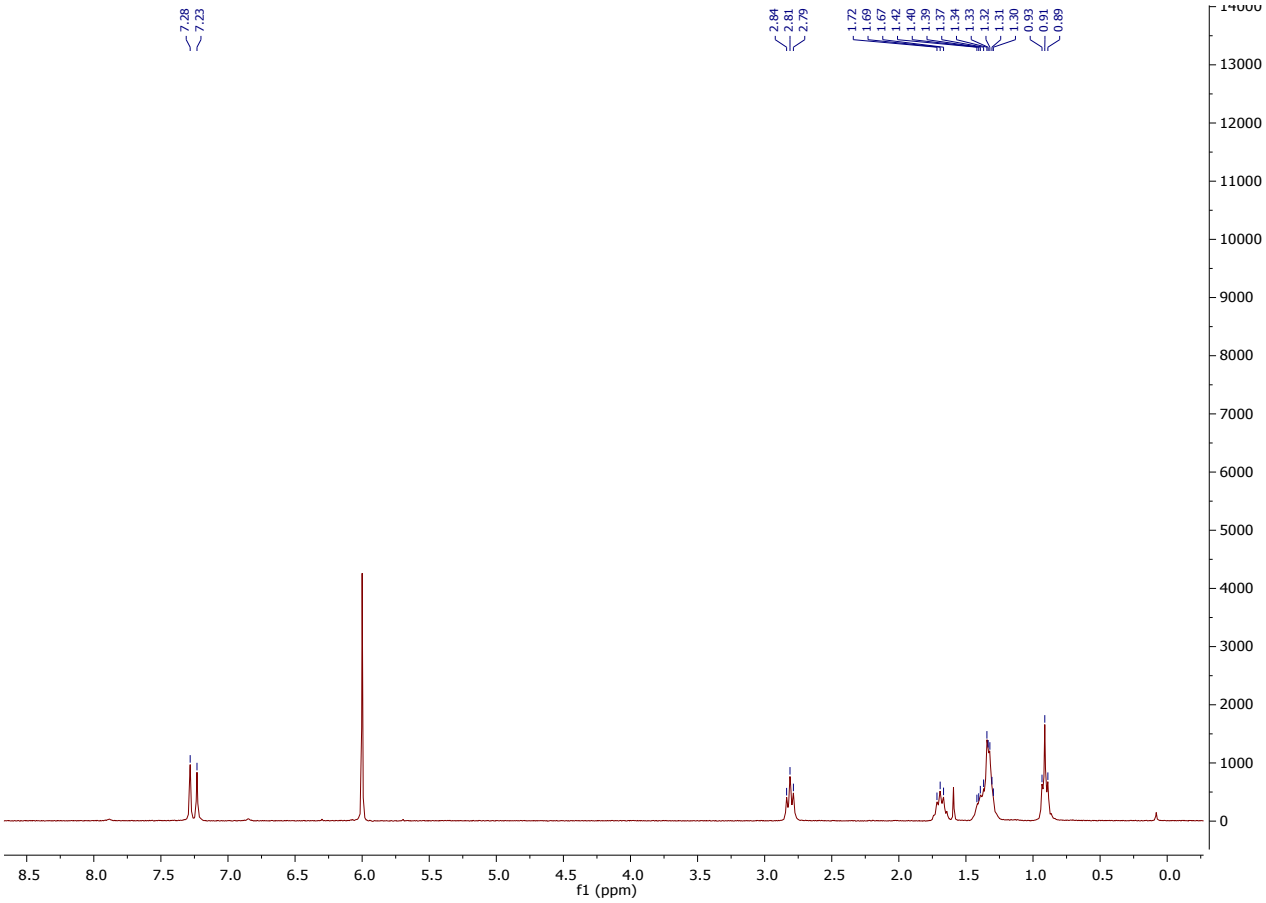

Figure S 22: ^{1}H NMR spectrum of ***para*-IDT(=NCN)$_2$** (1,1,2,2-Tetrachloroethane-d2)

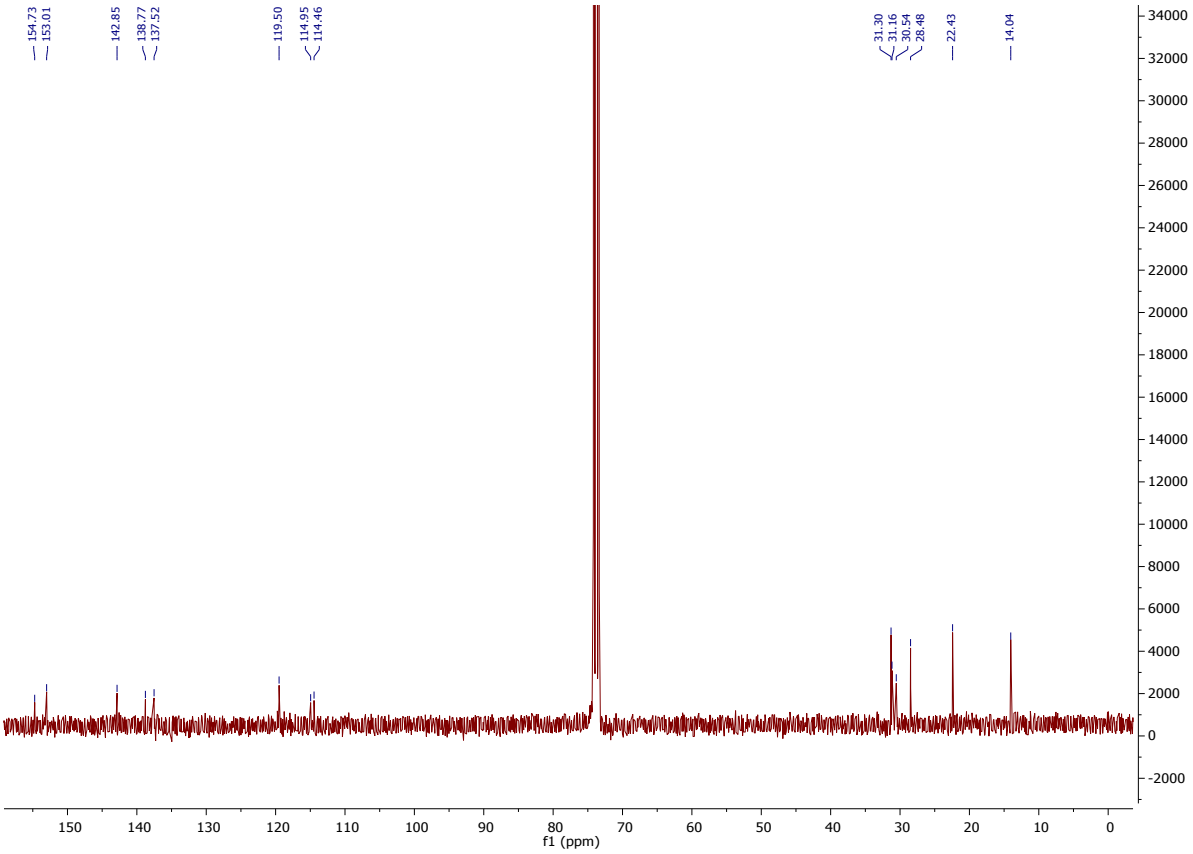

Figure S 23: ^{13}C NMR spectrum of ***para*-IDT(=NCN)$_2$** (1,1,2,2-Tetrachloroethane-d2)

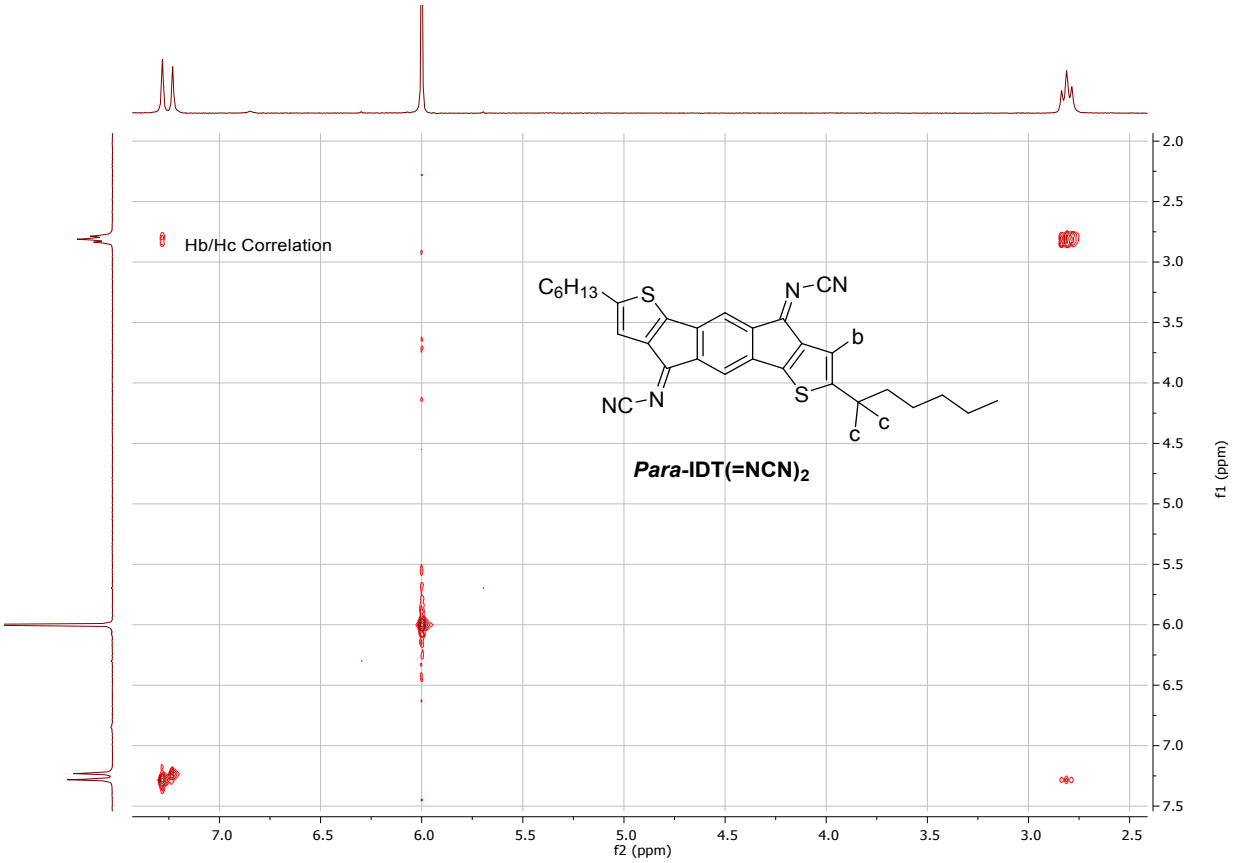

Figure S 24: Portion of the COSY spectrum of ***para*-IDT(=NCN)$_2$** (1,1,2,2-Tetrachloroethane-d2) showing the Hb/Hc correlation

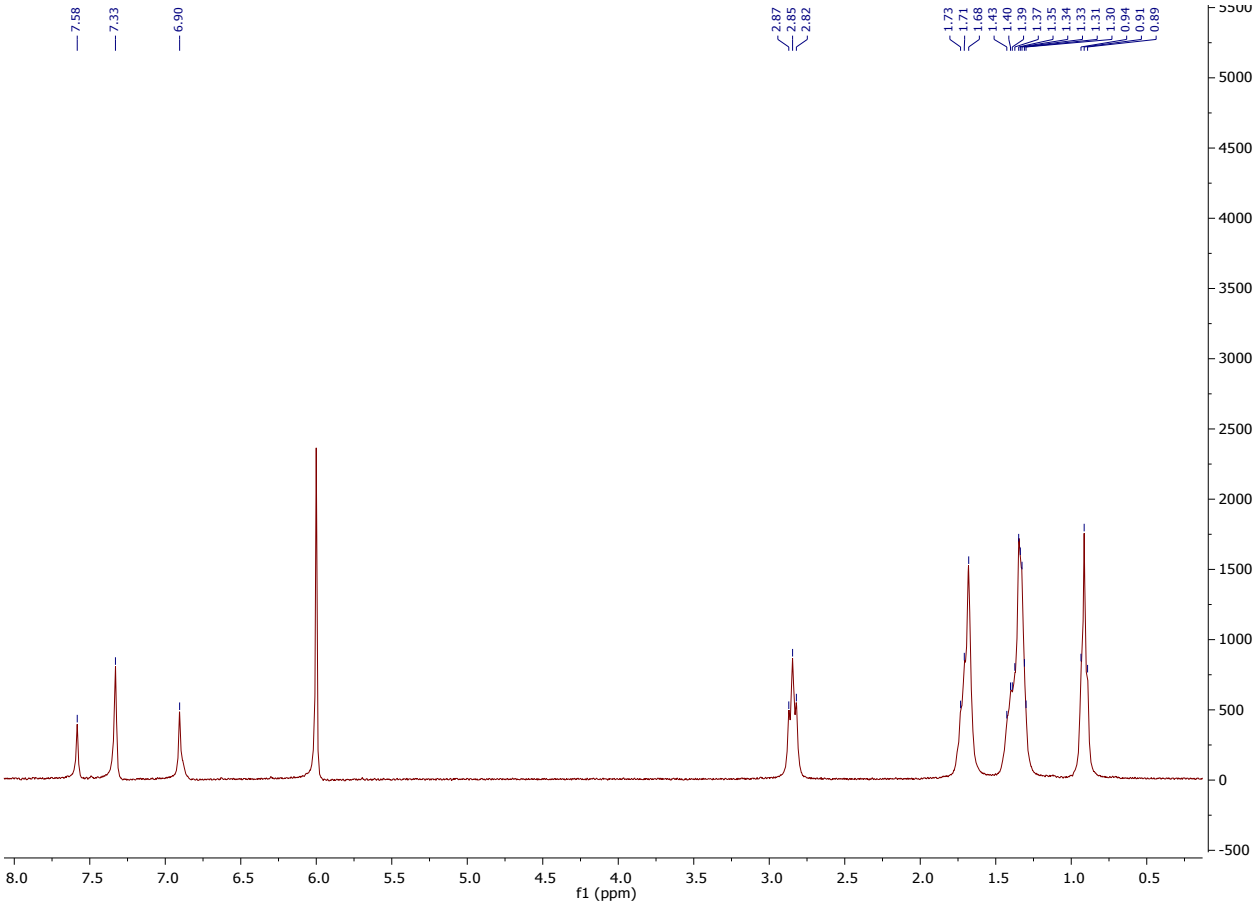

Figure S 25: ^{1}H NMR spectrum of ***meta*-IDT(=NCN)$_2$** (1,1,2,2-Tetrachloroethane-d2)

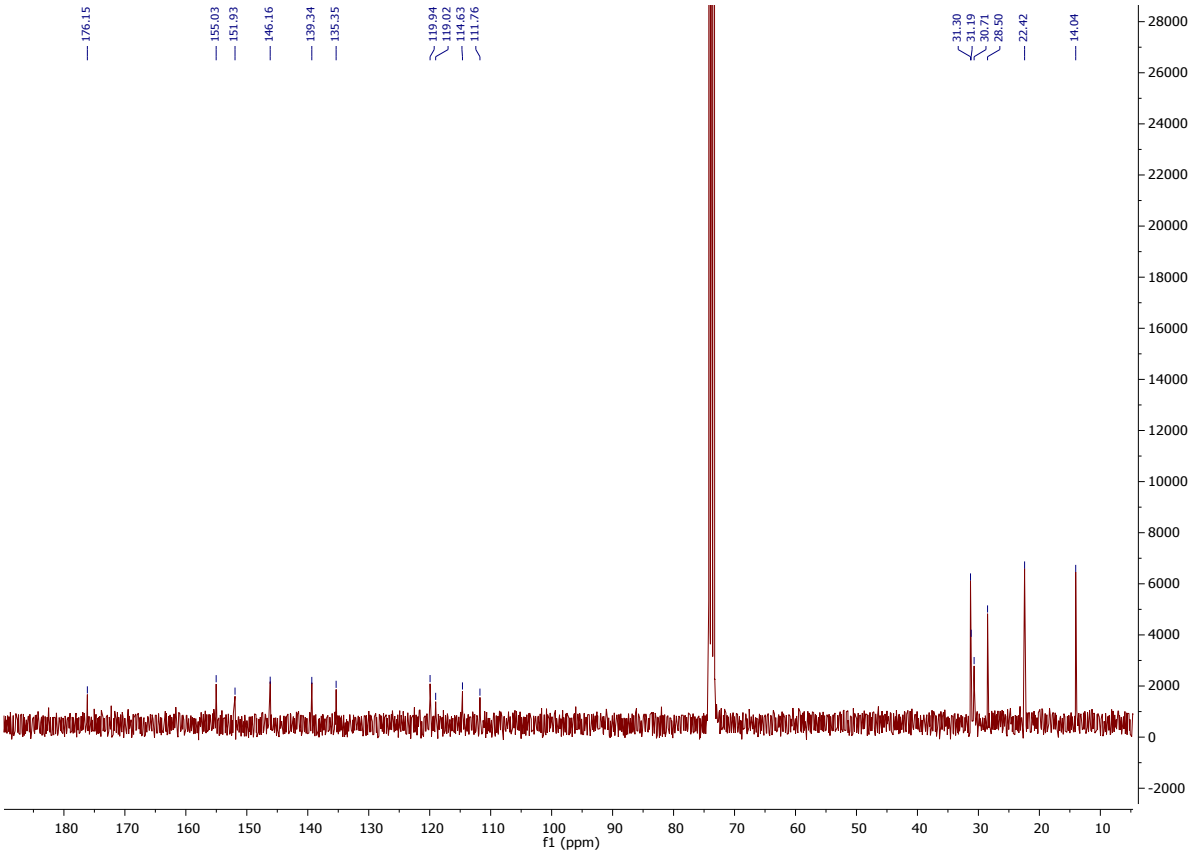

Figure S 26: ^{13}C NMR spectrum of ***meta*-IDT(=NCN)$_2$** (1,1,2,2-Tetrachloroethane-d2)

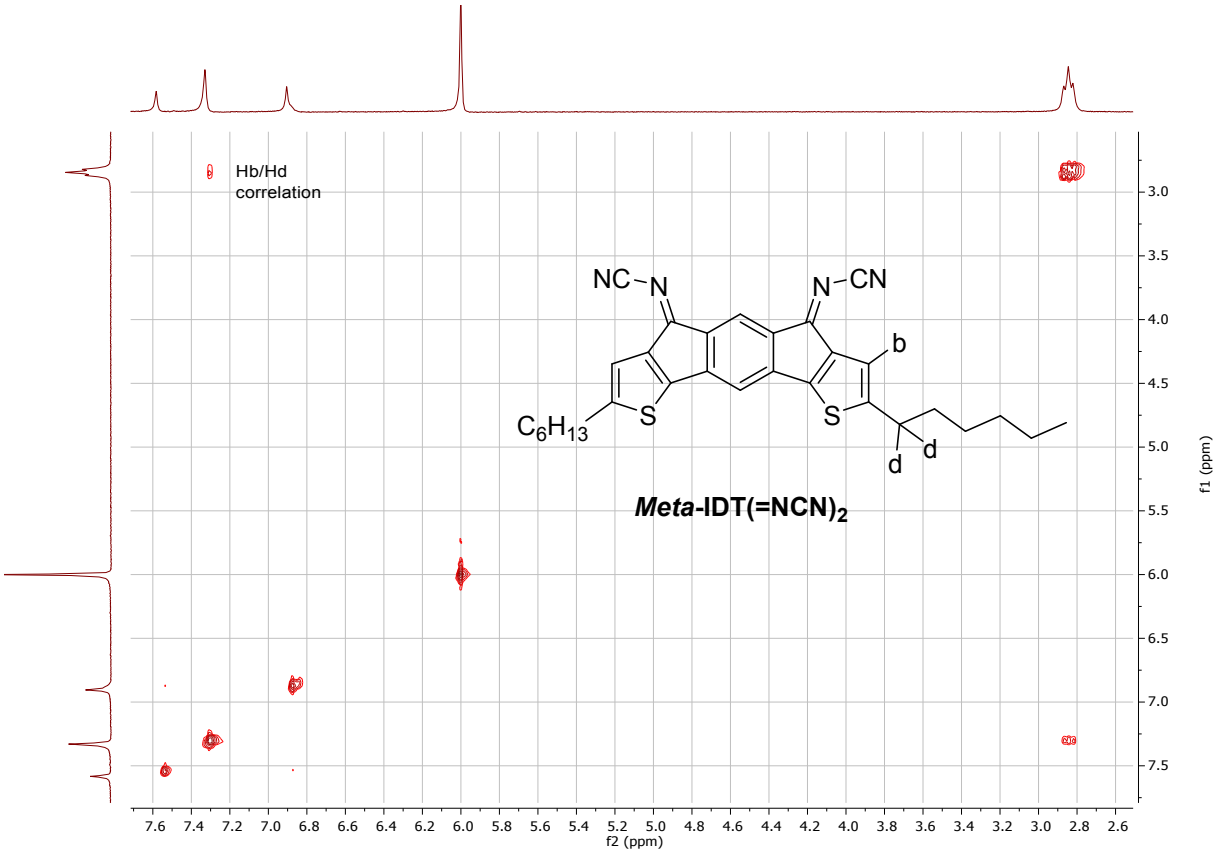

Figure S 27: Portion of the COSY spectrum of ***meta*-IDT(=NCN)$_2$** (1,1,2,2-Tetrachloroethane-d2) showing the Hb/Hc correlation

REFERENCES

1. Kulkarni, A. P.; Tonzola, C. J.; Babel, A.; Jenekhe, S. A., Electron Transport Materials for Organic Light-Emitting Diodes. *Chem. Mater.* **2004,** *16* (23), 4556–4573.
2. Hohenberg, P.; Kohn, W., Inhomogeneous Electron Gas. *Phys. Rev.* **1964,** *136*, B864-B871.
3. Calais, J.-L., Book Review. *Int. J. Quantum Chem.* **1993,** *47*, 101.
4. Becke, A. D., Density-functional exchange-energy approximation with correct asymptotic behavior. *Phys. Rev. A* **1988,** *38*, 3098-3100.
5. Becke, A. D., Density-functional thermochemistry. III. The role of exact exchange. *J. Chem. Phys.* **1993,** *98*, 5648 –5652.
6. Becke, A. D., A new mixing of Hartree–Fock and local density-functional theories. *J. Chem. Phys.* **1993,** *98*, 1372-1377.
7. Lee, C.; Yang, W.; Parr, R. G., Development of the Colle-Salvetti correlation-energy formula into a functional of the electron density. *Phys. Rev. B* **1988,** *37*, 785-789.
8. Frisch, M. J.; Trucks, G. W.; Schlegel, H. B.; Scuseria, G. E.; Robb, M. A.; Cheeseman, J. R.; Scalmani, G.; Barone, V.; Mennucci, B.; Petersson, G. A.; Nakatsuji, H.; Caricato, M.; Li, X.; Hratchian, H. P.; Izmaylov, A. F.; Bloino, J.; Zheng, G.; Sonnenberg, J. L.; Hada, M.; Ehara, M.; Toyota, K.; Fukuda, R.; Hasegawa, J.; Ishida, M.; Nakajima, T.; Honda, Y.; Kitao, O.; Nakai, H.; Vreven, T.; Montgomery, J. A. J.; Peralta, J. E.; Ogliaro, F.; Bearpark, M.; Heyd, J. J.; Brothers, E.; Kudin, K. N.; Staroverov, V. N.; Keith, T.; Kobayashi, R.; Normand, J.; Raghavachari, K.; Rendell, A.; Burant, J. C.; Iyengar, S. S.; Tomasi, J.;

Cossi, M.; Rega, N.; Millam, J. M.; Klene, M.; Knox, J. E.; Cross, J. B.; Bakken, V.; Adamo, C.; Jaramillo, J.; Gomperts, R.; Stratmann, R. E.; Yazyev, O.; Austin, A. J.; Cammi, R.; Pomelli, C.; Ochterski, J. W.; Martin, R. L.; Morokuma, K.; Zakrzewski, V. G.; Voth, G. A.; Salvador, P.; Dannenberg, J. J.; Dapprich, S.; Daniels, A. D.; Farkas, O.; Foresman, J. B.; Ortiz, J. V.; Cioslowski, J.; Fox, D. J., *Gaussian 09, Revision B.01; Gaussian, Inc.: Wallingford, CT, 2010.*

9. Janiak, C., A critical account on π–π stacking in metal complexes with aromatic nitrogen-containing ligands. *J. Chem. Soc., Dalton Trans.* **2000,** *21*, 3885-3896.

10. Yang, X.-J.; Drepper, F.; Wu, B.; Sun, W.-H.; Haehnel, W.; Janiak, C., From model compounds to protein binding: syntheses, characterizations and fluorescence studies of [RuII(bipy)(terpy)L]2+ complexes (bipy = 2,2[prime or minute]-bipyridine; terpy = 2,2[prime or minute]:6[prime or minute],2[double prime]-terpyridine; L = imidazole, pyrazole and derivatives, cytochrome c). *Dalton Trans.* **2005,** (2), 256-267.

11. Emma, C.; Cungen, Z.; Christoph, J.; Gerd, R.; Heinrich, L., Synthesis, Structure and Solution Chemistry of (5, 5′-Dimethyl-2, 2′-bipyridine)(IDA)copper(II) and Structural Comparison With Aqua(IDA)(1, 10-phenanthroline)copper(II) (IDA = iminodiacetato). *Zeitschrift für anorganische und allgemeine Chemie* **2003,** *629* (12-13), 2282-2290.

12. Banerjee, S.; Ghosh, A.; Wu, B.; Lassahn, P.-G.; Janiak, C., Polymethylene spacer regulated structural divergence in cadmium complexes: Unusual trigonal prismatic and severely distorted octahedral coordination. *Polyhedron* **2005,** *24* (5), 593-599.

13. Dorn, T.; Janiak, C.; Abu-Shandi, K., Hydrogen-bonding, π-stacking and Cl−-anion–π interactions of linear bipyridinium cations with phosphate, chloride and [CoCl4]2− anions. *CrystEngComm* **2005,** *7* (106), 633-641.

14. MicroChem SU-8 2000 Permanent Epoxy Negative Photoresist Processing guidelines for SU-8 2000.5, SU-8 2002, SO-8 2005, SU-8 2007, SU-8 2010 and SU-8 2015. http://www.microchem.com/pdf/SU-82000DataSheet2000_5thru2015Ver4.pdf.